JACS
JOURNAL OF THE AMERICAN CHEMICAL SOCIETY
pubs.acs.org/JACS
Article

Reversible Modulation of the Electronic and Spatial Environment around Ni(0) Centers Bearing Multifunctional Carbene Ligands with Triarylaluminum

Yasuhiro Yamauchi, Yutaka Mondori, Yuta Uetake,* Yasuo Takeichi, Takahiro Kawakita, Hidehiro Sakurai, Sensuke Ogoshi,* and Yoichi Hoshimoto*

Cite This: J. Am. Chem. Soc. 2023, 145, 16938−16947
Read Online

ACCESS | Metrics & More | Article Recommendations | Supporting Information

ABSTRACT: Designing and modulating the electronic and spatial environments surrounding metal centers is a crucial issue in a wide range of chemistry fields that use organometallic compounds. Herein, we demonstrate a Lewis-acid-mediated reversible expansion, contraction, and transformation of the spatial environment surrounding nickel(0) centers that bear *N*-phosphine oxide-substituted *N*-heterocyclic carbenes (henceforth referred to as (S)PoxIms). Reaction between tetrahedral (*syn*-κ-*C*,*O*-(S)PoxIm)-Ni(CO)$_2$ and Al(C$_6$F$_5$)$_3$ smoothly afforded heterobimetallic Ni/Al species such as trigonal-planar {κ-*C*-Ni(CO)$_2$}(*μ*-*anti*-(S)PoxIm)-{κ-*O*-Al(C$_6$F$_5$)$_3$} via a complexation-induced rotation of the *N*-phosphine oxide moieties, while the addition of 4-dimethylaminopyridine resulted in the quantitative regeneration of the former Ni complexes. The corresponding interconversion also occurred between (SPoxIm)Ni(η^2:η^2-diphenyldivinylsilane) and {κ-*C*-Ni(η^2:η^2-diene)}(*μ*-*anti*-SPoxIm){κ-*O*-Al(C$_6$F$_5$)$_3$} via the coordination and dissociation of Al(C$_6$F$_5$)$_3$. The shape and size of the space around the Ni(0) center was drastically changed through this Lewis-acid-mediated interconversion. Moreover, the multinuclear NMR, IR, and XAS analyses of the aforementioned carbonyl complexes clarified the details of the changes in the electronic states on the Ni centers; i.e., the electron delocalization was effectively enhanced among the Ni atom and CO ligands in the heterobimetallic Ni/Al species. The results presented in this work thus provide a strategy for reversibly modulating both the electronic and spatial environment of organometallic complexes, in addition to the well-accepted Lewis-base-mediated ligand-substitution methods.

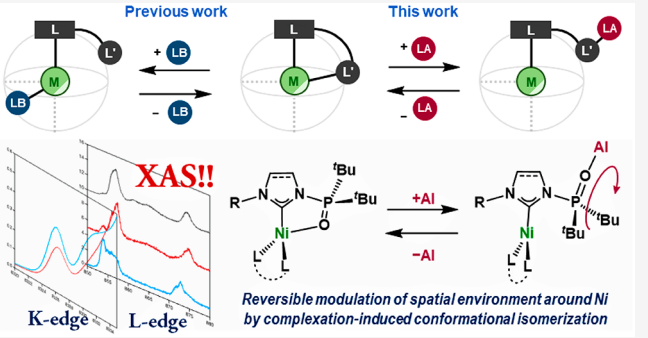

INTRODUCTION

Designing the spatial environment around a metal center is a critical issue in terms of the electronic and steric properties and hence the reactivity of organometallic complexes. Chemists have thus focused on the design of the structural, electronic, and dynamic properties of supported ligands, as demonstrated in the field of, e.g., homogeneous catalysis,[1−6] supramolecular chemistry,[7,8] and materials science.[9] One well-known strategy for reversibly modulating the electronic and spatial environment around metal centers is based on a ligand-substitution process on metal centers bearing multifunctional ligands including a hemilabile coordination moiety (L′) in the presence of an external Lewis base (LB) (Figure 1A, left).[10−14] However, these processes often yield an equilibrium mixture that is difficult to separate. In this context, we have reported the reversible, recyclable, and pressure-responsive room-temperature-chemisorption of carbon monoxide (CO) on a zerovalent nickel complex that bears multifunctional multipurpose carbene ligands,[14] namely *N*-phosphine oxide-substituted imidazolinylidenes (SPoxIms) and the corresponding imidazolylidenes (PoxIms) (Figure 1B, left).[15,16] (S)PoxIm ligands in tetrahedral (S)PoxImNi(CO)$_n$ complexes selectively adopt either a κ-*C*- (n = 3) or κ-*C*,*O*- (n = 2) coordination mode, which can be interconverted through the addition/exclusion of CO.

A strategy based on the use of Lewis acids (LAs) is another potential option for reversibly modulating the spatial environment around metal centers that bear multifunctional ligands (Figure 1A, right).[17−20] The LA-mediated process can cause a substantial change in both the electronic state and spatial environment of the metal center due to the change in the number of ligands. This feature clearly distinguishes LA-mediated processes from LB-mediated ones as the latter commonly proceeds without changing the number of ligands.

Received: June 14, 2023
Published: July 19, 2023

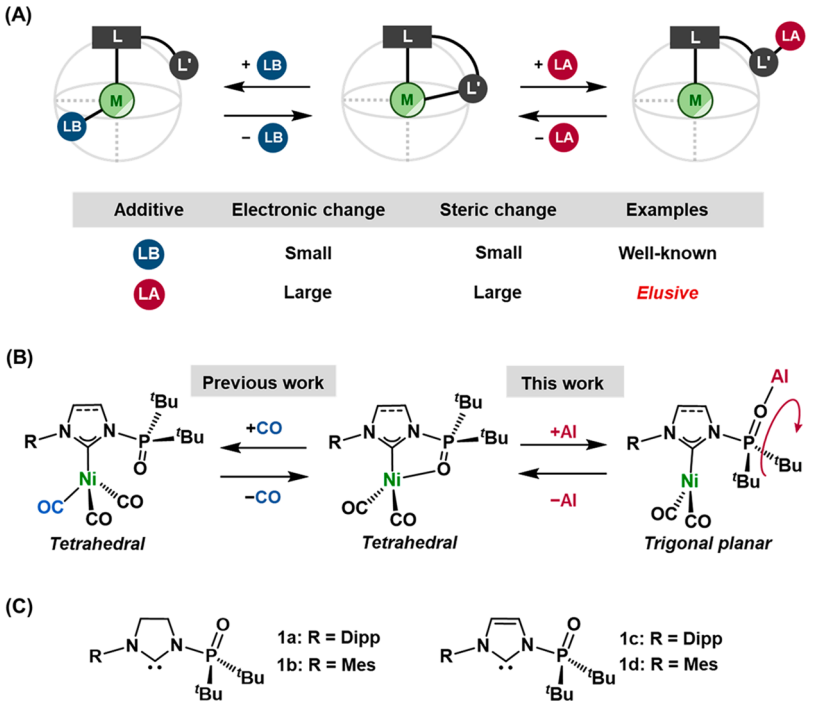

Figure 1. (A) A simplified scheme of the reversible modulation of the spatial environment around a metal center in an organometallic complex mediated by Lewis bases (LBs, left) or Lewis acids (LAs, right). (B) Reversible transformation of Ni/(S)PoxIm complexes using Lewis-basic CO (our previous work, left) and Lewis-acidic aluminum species (this work, right). (C) The (S)PoxIms used in this work (Dipp = 2,6-diisopropylphenyl, Mes = 2,4,6-trimethylphenyl).

However, examples of such LA-mediated reactions have been severely limited because LAs often trigger the irreversible decomposition of the organometallic complex via the abstraction of ligands to form an LA–LB adduct. A judicious combination of multifunctional ligands and LAs is thus essential for constructing an LA-mediated system that can reversibly regulate the electronic and spatial environments around the metal centers. It should be noted that Fan et al. have reported an example that relies predominantly on an electrostatic interactions[21,22] involving the reversible complexation of Na^+ and a crown-ether moiety included in a Rh complex that bears Aza-CrownPhos; the reactivity of the Rh complex can be regulated through the Na^+-mediated interconversion.[23] The authors evaluated the change in the spatial environment around the Rh center using multinuclear NMR spectroscopy and ESI mass spectrometry, even though a quantitative evaluation of how much the field expanded and diminished via the reaction was not discussed.

Herein, we present a novel strategy to reversibly transform the spatial environment around a nickel center by combining (S)PoxIms **1a–d** (Figure 1C) as multifunctional ligands and tris(pentafluorophenyl)aluminum as an LA, where the geometry of the Ni center is interconverted between tetrahedral and trigonal planar (Figure 1B, right). We quantitatively evaluated the variation of the spatial environment, i.e., the volume and shape of the space, and the electronic state around the nickel center based on single-crystal X-ray diffraction (SC-XRD) and X-ray absorption spectroscopy (XAS) analyses.

RESULTS AND DISCUSSION

Previously, we have reported that (S)PoxIms include *syn*- and *anti*-conformers with respect to the N–P bonds, which can interconvert easily at room temperature via rotation of the *N*-phosphinoyl groups ($\Delta E^{\ddagger} \sim 12$ kcal mol^{-1} for previously reported PoxIms), even though the *anti*-conformers are thermodynamically favorable (Figure 2).[15,16] Importantly, the

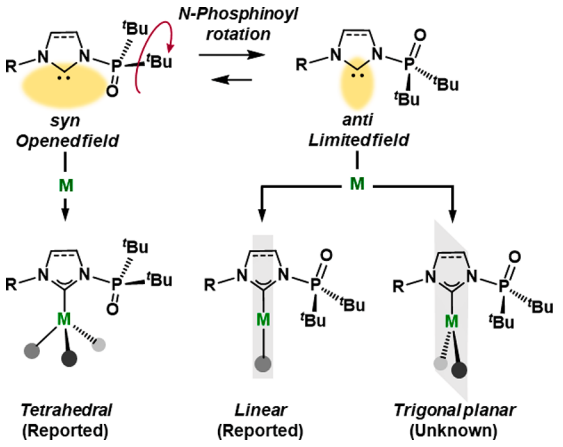

Figure 2. Interconversion between *syn*- and *anti*-conformers of (S)PoxIms, as well as complexation between (S)PoxIms and transition metals that prefer different coordination geometries.

volume and shape of the space can be drastically varied via rotation of the *N*-phosphinoyl groups, and a relatively limited space is present around the carbene carbon atoms in the *anti*-(S)PoxIms. Due to this limited spatial environment, only group-11 metals such as Cu[24] and Au[25] have been confirmed to form complexes that bear *anti*-(S)PoxIms in a *κ-C* fashion, given that these metals tend to adopt two-coordinated linear complexation geometries (Figure 2). We have also reported the synthesis of heterobimetallic complexes of the type (*κ-C*-

https://doi.org/10.1021/jacs.3c06267
J. Am. Chem. Soc. 2023, 145, 16938–16947

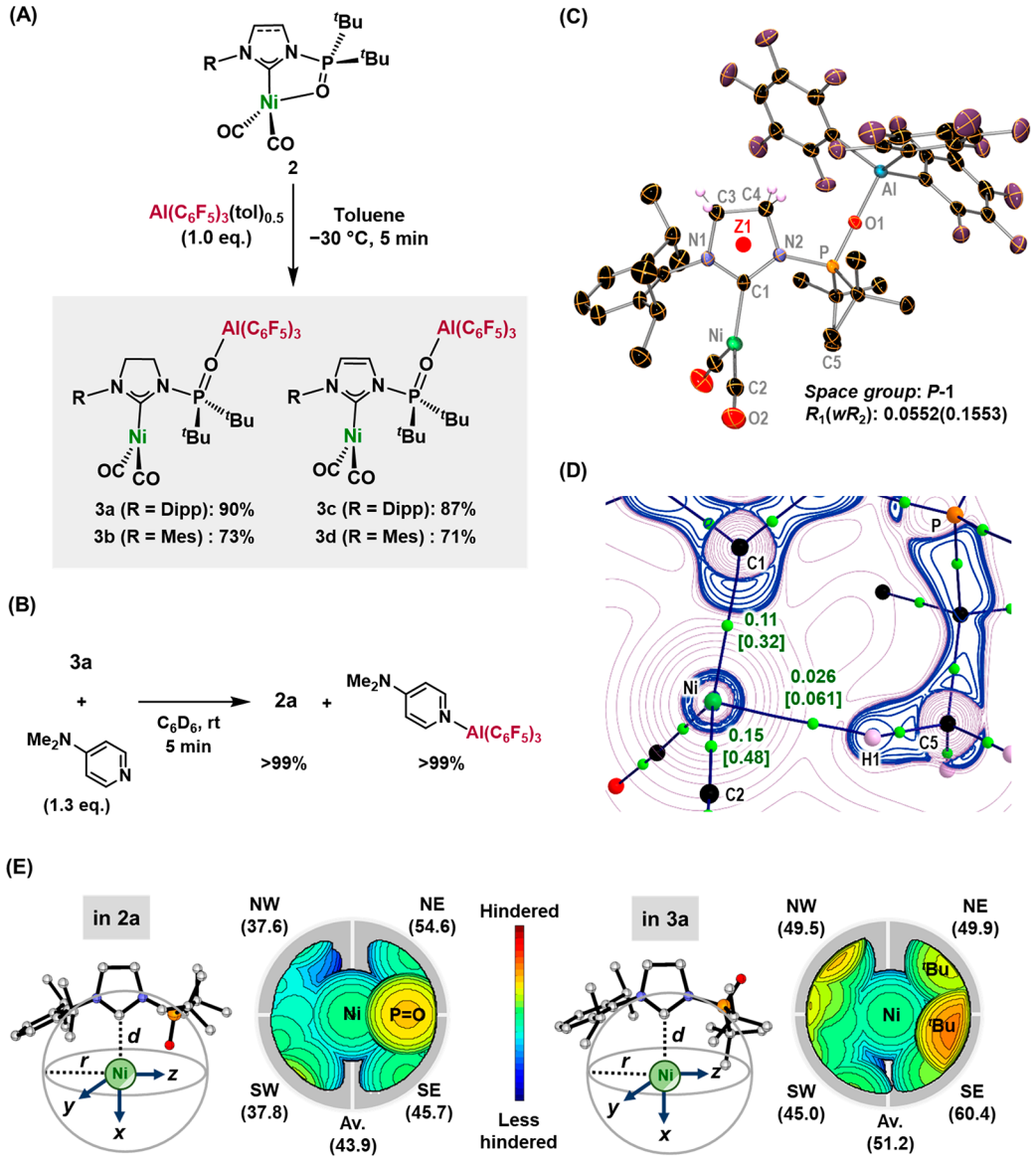

Figure 3. (A) Synthesis of the heterobimetallic Ni/Al complexes **3** via the reaction between (*syn*-κ-*C*,*O*-**1**)Ni(CO)$_2$ (**2**) and an equimolar amount of Al(C$_6$F$_5$)$_3$(tol)$_{0.5}$. Yield of isolated products is shown. (B) Reaction of **3a** with DMAP. (C) Molecular structure of **3a** with a thermal ellipsoid at 30% probability; H atoms (except those bound to C3 and C4) are omitted for clarity. Selected bond lengths (Å) and angles (deg): Ni−C1 1.945(3), Ni−C2 1.759(3), Ni−C5 3.240(4), C2−O2 1.140(4), P−O1 1.524(2), O1−Al 1.799(2), Z1−C1−Ni 169.9, C1−N2−P−O1 159.7(2). (D) The quantum theory of AIM bond paths (black lines) and bond-critical points (green dots) are overlaid with the contour plots of $\nabla^2\rho$ through the plane defined by the C1, Ni, and C5 atoms. Selected atoms and values of the electron density ($e\ r_{Bohr}^{-3}$) are shown. The values of $\nabla^2\rho$ ($e\ r_{Bohr}^{-5}$) are shown in square brackets. (E) Topographic steric maps and %V_{bur} values of **2a**/**3a** calculated using the program SambVca (r = 3.5 Å; d = 2.0 Å; bond radii scaled by 1.17; mesh spacing 0.05; H atoms are omitted) based on the structural parameters obtained from the SC-XRD analysis.

Cu)(*μ-anti*-(S)PoxIm)(κ-*O*-Al) through complexation between *anti*-(κ-*O*-(S)PoxIm)Al(C$_6$F$_5$)$_3$ and CuO^{t}Bu followed by an irreversible intramolecular Cu−O^{t}Bu/Al−C$_6$F$_5$ transmetalation triggered by the rotation of the *N*-phosphinoyl moiety.[24] However, reversible spatial modifications around the metal center between isolable species remain challenging.

In this work, we envisioned an Al(C$_6$F$_5$)$_3$-mediated reversible interconversion between complexes bearing *syn*- and *anti*-(S)PoxIms based on the use of Ni(0), i.e., an interconversion between tetrahedral (κ-*C*,*O*-(S)PoxIm)Ni(CO)$_2$ and trigonal-planar {κ-*C*-Ni(CO)$_2$}(*μ-anti*-(S)PoxIm)-{κ-*O*-Al(C$_6$F$_5$)$_3$} (Figure 1B, right). The preparation of trigonal-planar Ni(0) dicarbonyl complexes that bear bulky *N*-heterocyclic carbenes (NHCs) such as (I^{t}Bu)Ni(CO)$_2$ and (IAd)Ni(CO)$_2$[26,27] (I^{t}Bu = 1,3-di-*tert*-butylimidazol-2-ylidene; IAd = 1,3-diadamantylimidazol-2-ylidene) has already been reported, which inspired us to explore the preparation of Ni(0) complexes bearing bulky *anti*-(S)PoxIm ligands (Figure 2).

We started our study with the reaction between (*syn*-κ-*C*,*O*-**1a**)Ni(CO)$_2$ (**2a**) and an equimolar amount of Al(C$_6$F$_5$)$_3$(tol)$_{0.5}$, which resulted in the selective formation of heterobimetallic Ni/Al complex **3a** in 90% yield (Figure 3A). We also confirmed that the Al(C$_6$F$_5$)$_3$-mediated rotation of *N*-phosphinoyl moieties in **2b**−**d** afforded the corresponding heterobimetallic Ni/Al complexes (**3b**−**d**) in good-to-high yield. The differences in steric bulkiness between the Dipp and

https://doi.org/10.1021/jacs.3c06267
J. Am. Chem. Soc. 2023, 145, 16938−16947

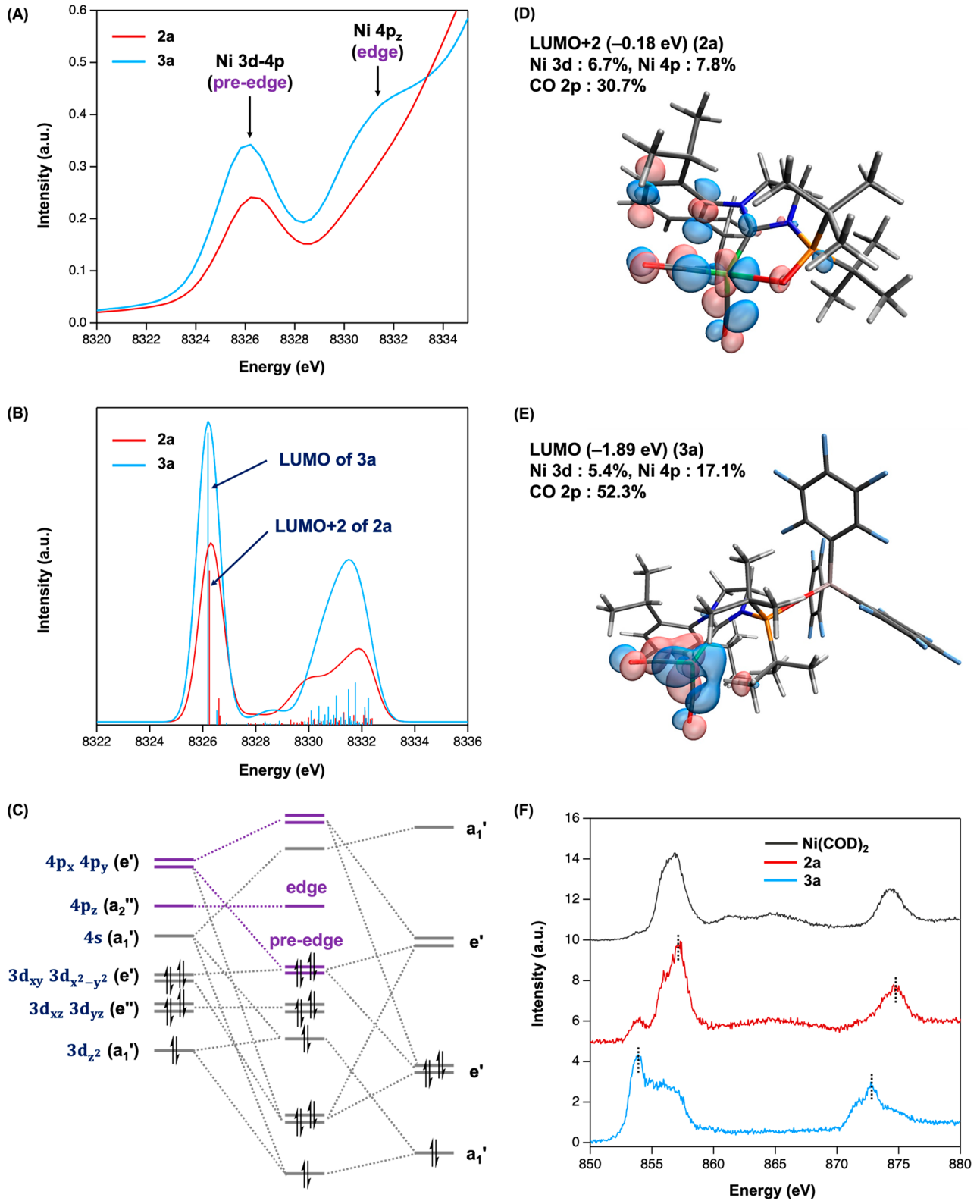

Figure 4. (A) Ni K-edge XANES spectra of **2a**/**3a** in toluene. (B) The simulated Ni K-edge XAS spectra of **2a**/**3a** using the TDDFT method at the ZORA-B3LYP/CP(PPP) (for Ni) and ZORA-def2-TZVP(-f) (for C, H, O, N, F, P, and Al) level. (C) Qualitative MO diagram of the trigonal-planar complex. The purple bars denote electric dipole allowed, and the gray bars forbidden transition orbitals in the Ni K-edge XAS. (D) Kohn–Sham LUMO+2 for **2a**. (E) Kohn–Sham LUMO for **3a**. (F) Ni $L_{2,3}$-edge XAS spectra of $Ni(cod)_2$, **2a**, and **3a** in the PFY method.

Mes groups, as well as the structural flexibility variations between saturated SPoxIms and unsaturated PoxIms, had no significant effect on the progress of the reaction. The molecular structures of **3a**–**d** were fully characterized using NMR and ATR-infrared (IR) absorption spectroscopy as well as SC-XRD analysis (*vide infra*). Subsequently, we treated **3a** with slight excess amounts of 4-dimethylaminopyridine (DMAP) and confirmed the quantitative regeneration of **2a** with the

https://doi.org/10.1021/jacs.3c06267
J. Am. Chem. Soc. 2023, 145, 16938–16947

concomitant formation of the adduct DMAP−Al(C_6F_5)$_3$ (Figure 3B). These results demonstrated that the interconversion between **2a** and **3a** can be successfully mediated by the addition and removal of Al(C_6F_5)$_3$.

Next, we compared the electronic and geometric parameters of **2a** and **3a**. In the ^{31}P NMR spectrum of **3a**, the resonance corresponding to the *N*-phosphinoyl moiety is observed at δ_P 82.0 in toluene-d_8, which represents a significant downfield shift compared to that of **2a** (δ_P 68.0 in THF-d_8),[14] while it is almost identical to that of (κ-*O*-**1a**)Al(C_6F_5)$_3$ (δ_P 79.8 in CD_2Cl_2).[24] These results indicate that the **1a** moiety in **3a** should predominantly adopt the *anti*-conformation. The geometric parameters of **3a** obtained from the SC-XRD analyses are shown in Figure 3C. As previously reported, the Ni center in **2a**, which bears the κ-*C*,*O*-*syn*-**1a** ligand (C−N−P−O torsion angle: 8.5(1)°), adopts a tetrahedral geometry.[14] In stark contrast, **3a** features a trigonal-planar Ni center (sum of bond angles around Ni: 358.9°) bearing *anti*-**1a** (C1−N2−P−O1 torsion angle: 159.7(2)°),[28] as shown in Figure 3C. The Ni(CO)$_2$ unit is located slightly out of ideal alignment with the carbene lone pair (Z1−C1−Ni angle: 169.9°; Z1 = centroid of the imidazolinylidene ring), most likely due to the high steric demand of the ^{t}Bu groups.

Interestingly, a noncovalent interaction between the Ni and H1 atoms was confirmed in the gas-phase-optimized structure of **3a** (level: PBE0/def2-TZVPD//M06L/def2-SVPD for O, F, and Ni; def2-SVP for all other atoms) via a topological analysis of the electron density, which was calculated using the quantum theory of atoms in molecule (AIM) method (Figure 3D).[29,30] It should also be noted here that the geometric parameters of the solid state structure of **3a** confirmed by SC-XRD analysis were closely reproduced in the theoretically calculated gas-phase-optimized structure; e.g., the interatomic distances between the Ni and C5 atoms were 3.18 Å in the gas-phase and 3.240(4) Å in the crystalline state. In fact, the Ni···H1 distance (2.13 Å)[31] and the relatively high electron density (ρ = 0.026 e r_{Bohr}^{-3}) as well as the positive value of the Laplacian of the electron density ($\nabla^2\rho$ = +0.061 e r_{Bohr}^{-5}) at the bond-critical point (BCP) between these atoms suggests the participation of an agostic Ni···H interaction.[29,30]

Dissociation of the *N*-phosphinoyl moiety from tetrahedral **2a** to afford trigonal planar **3a** also caused obvious changes in the wavenumbers of the stretching vibration of the CO ligands. In fact, the signal corresponding to the stretching vibration of the CO ligands in **3a** was observed at 2019 cm^{-1}, i.e., at a higher wavenumber than that of **2a** (1967 cm^{-1}). The AIM analysis clarifies the increase in the delocalization indices δ(Ni, C_{CO}) and δ(Ni, O_{CO}) in **3a** compared to those in **2a**, which represent a number of electron pairs delocalized between the Ni and carbonyl carbon atoms (C_{CO}) and the Ni and carbonyl oxygen atoms (O_{CO}), respectively (Figures S7−S8).[30] The mean values of δ(Ni, C_{CO}) and δ(Ni, O_{CO}) increase from 0.51 (**2a**) to 1.20 (**3a**) and from 0.063 (**2a**) to 0.23 (**3a**), respectively, indicating that electrons become effectively delocalized through the Ni, C_{CO}, and O_{CO} atoms in **3a**. On the other hand, the values of δ(C_{CO}, O_{CO}) are nearly identical between **2a** (1.70−1.71) and **3a** (1.60−1.62). Thus, we attribute the aforementioned blue-shift to the increased polarization of the π CO bonding orbitals due to an increased cationic nature on the Ni in **3a** (AIM atomic net charge = 0.50 e) compared to **2a** (AIM atomic net charge = −0.1 e).[32]

Based on the aforementioned geometric parameters of **2a** and **3a** in the crystalline state, the impact of the *N*-phosphinoyl rotation on the spatial environment surrounding the Ni center was quantitatively evaluated on the basis of percent buried volume (%V_{bur}) (Figure 3E).[2,33] Topographic steric maps that visualize the %V_{bur} values in the northwestern (NW), northeastern (NE), southwestern (SW), and southeastern (SE) quadrants, as well as their average (Av), are also depicted; these maps were produced using the program Samb*V*ca. 2.1.[2] The Av(%V_{bur}) values in **2a** and **3a** were calculated to be 43.9 and 51.2, respectively, clearly demonstrating that the space around the Ni center is significantly altered via rotation of the *N*-phosphinoyl moiety. Importantly, drastic expansion/contraction of the space can be precisely and reversibly triggered by the addition/removal of Al(C_6F_5)$_3$. In addition, this rotational transformation alters the shape of the space around the Ni center, as is clearly confirmed by the comparison of both the %V_{bur}(NE) and %V_{bur}(SE) values of **2a** and **3a**.

We then carried out solution-phase XAS measurements to determine whether the results obtained from the SC-XRD analysis could be extended to the solvated states of **2a** and **3a**. A magnified view of the pre-edge and edge region of the Ni K-edge X-ray absorption near edge structure (XANES) is shown in Figure 4A. In the case of **2a**, a pre-edge peak corresponding to the electric dipole transition from the Ni 1s orbital to the Ni 4p(−3d) orbitals was observed at 8326 eV and no characteristic peak was detected at the absorption edge, which is typical for nickel complexes with tetrahedral geometry.[14] Meanwhile, a remarkable peak appeared in the edge region (8331 eV) for **3a**, along with a greater pre-edge peak intensity compared to **2a**. We attribute the characteristic edge peak to the Ni 1s → 4p$_z$ transition in **3a**, given the presence of the nonbonding 4p$_z$ orbital (a_2'' symmetry) (Figure 4C). Considering that such nonbonding 4p$_z$ orbitals are commonly found in trigonal-planar 16-electron complexes, the results of the solution-phase XAS experiments clearly rationalize the adoption of a trigonal-planar geometry by **3a**, even in toluene, as observed in the crystal structure.

To gain further insight, the Ni K-edge XAS spectra of **2a** and **3a** were simulated using the time-dependent DFT (TDDFT) calculation at the B3LYP level with the zeroth-order regular approximation (ZORA)[34−36] to take the relativistic effect into consideration.[37] The CP(PPP) basis set was used for Ni, while the ZORA-def2-TZVP(-f) basis set was used for all of the other elements. The intensities of the pre-edge and edge peaks of the simulated XAS spectra show good agreement with those of the experimental spectra (Figure 4A and 4B). To identify the predominant contribution to the pre-edge peaks, we then analyzed the molecular orbitals (MOs) of **2a** and **3a**. In the case of **2a**, the transition from the Ni 1s orbital to LUMO+2 significantly contributes to the pre-edge peak, where LUMO+2 mainly consists of the Ni 3d (6.7%), Ni 4p (7.8%), and CO 2p (30.7%) orbitals (Figure 4D). On the other hand, in the case of **3a**, the increased intensity of the corresponding pre-edge peak can be rationalized predominantly by the transition from the Ni 1s orbital to the LUMO. The LUMO of **3a** features increased contribution from the Ni 4p orbitals (17.1%) and CO ligands (52.3%) compared to their contributions to the LUMO+2 in **2a** (Figure 4E), while the Ni 3d orbitals exhibit a nearly identical degree of contribution to the respective MOs in **2a** and **3a**. We therefore attributed the increase in the pre-edge peak intensity of **3a** induced by the Al(C_6F_5)$_3$-mediated geometric change to the increased efficiency of the Ni 3d−4p mixing and contribution of CO ligands (e′ symmetry) in the trigonal planar geometry.

https://doi.org/10.1021/jacs.3c06267
J. Am. Chem. Soc. 2023, 145, 16938−16947

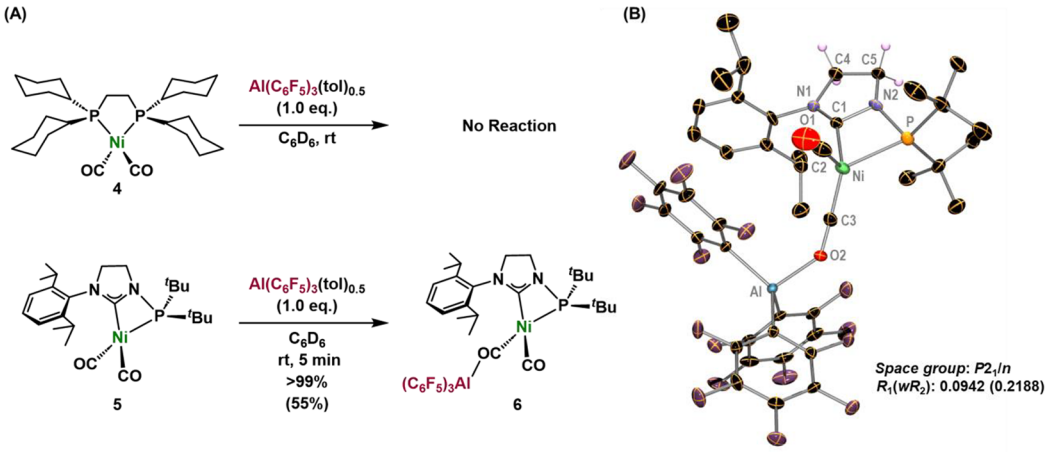

Figure 5. (A) Reactions between complexes **4** and **5** and $Al(C_6F_5)_3(tol)_{0.5}$. The yield was determined by NMR analysis. The yield of isolated products is shown in parentheses. (B) Molecular structure of **6** with thermal ellipsoids at 30% probability; H atoms (except those bound to C4 and C5) are omitted for clarity. Selected bond lengths (Å) and angles (deg): Ni−C1 1.991(6), Ni−P 2.314(2), Ni−C2 1.814(8), Ni−C3 1.691(5), C2−O1 1.12(1), C3−O2 1.197(6), O2−Al 1.861(4), and C3−O2−Al 139.3(4).

We further explored the electronic structures of the Ni 3d orbitals in the solid state for **2a** and **3a** based on Ni $L_{2,3}$-edge XAS experiments using the partial fluorescence yield (PFY) method. In the cases of **2a** and $Ni(cod)_2$, the absorption maxima on the Ni L_3-edge appear at 856.0 and 856.2 eV, respectively, with a shoulder peak in their lower-energy regions (Figure 4F). These Ni $L_{2,3}$-edge XAS spectra represent spectroscopic features characteristic of tetrahedral nickel complexes with a d^{10} electron configuration (formally Ni(0)). In contrast, for **3a**, the peak maximum shifts toward the lower-energy region to 852.9 eV, clearly indicating that the 3d orbitals are stabilized through the formation of the 16-electron complex with a vacant $4p_z$ orbital. In fact, the energy levels of the unoccupied frontier MOs of **3a** are substantially lower than those of **2a**, showing good agreement with the experimental Ni $L_{2,3}$-edge XAS data (Table S4). Furthermore, a broad signal is observed in the higher energy region at 854−858 eV. Based on the results of the Cu $L_{2,3}$-edge XAS experiments previously reported by Lancaster et al., we attribute this signal to the transitions from the Ni $2p_{3/2}$ orbital to the ligand and Ni 3d orbitals, given the occupied d^{10} electron configuration in **3a**.[37]

To clarify the key role of (S)PoxIms, we subsequently explored reactions between $Al(C_6F_5)_3$ and Ni(0) dicarbonyl complexes **4** and **5** (Figure 5A). Complex **4**, which carries the bis(dicyclohexylphosphino)ethane ligand, did not react with $Al(C_6F_5)_3$ under the applied conditions. On the other hand, **6** was quantitatively formed without complexation between the phosphine moiety and $Al(C_6F_5)_3$ when *N*-phosphanyl-substituted imidazolidine-2-ylidene was used as a hemilabile ligand instead of **1a**. The molecular structure of **6** was unambiguously determined by a SC-XRD analysis and is shown in Figure 5B. Even though our targeted spatial modulation was not confirmed, these results are noteworthy to demonstrate that CO ligands are sufficiently Lewis-basic to form classical Lewis-acid/base adducts with Lewis-acidic triarylaluminum species.[38−40] The aforementioned results suggest that to realize the $Al(C_6F_5)_3$-mediated reversible modulation of the spatial environment surrounding Ni(0) it is crucial to use a hemilabile ligand that includes both hard and soft (or mild) Lewis-basic sites and that is responsive to external stimuli in order to induce a preprogrammable structural isomerization. (S)PoxIms with their distinctive Lewis-basic sites, i.e., the harder phosphinoyl oxygen moiety and the softer carbene moiety, as well as the complexation-induced rotation of the *N*-phosphinoyl moiety may thus successfully serve as pioneering examples for this purpose.

Finally, we confirmed that the present strategy can be expanded to (*syn*-κ-*C*,*O*-**1a**)Ni complex **7a**, which contains an η^2:η^2-diphenyldivinylsilane ligand instead of CO (Figure 6A). Treatment of **7a** with $Al(C_6F_5)_3(tol)_{0.5}$ resulted in the quantitative formation of the heterobimetallic Ni/Al complex **8a** via the complexation-induced rotation of the *N*-phosphinoyl moiety. Moreover, the addition of DMAP again caused the dissociation of $Al(C_6F_5)_3$ to regenerate **7a**.

The molecular structures of compounds **7a** and **8a** were confirmed by SC-XRD analyses (Figure 6B). Although the C1−Ni lengths remained almost unchanged upon rotation of the *N*-phosphinoyl moiety, the sterically demanding ^{t}Bu groups cause a significant deviation of the Ni(η^2:η^2-diphenyldivinylsilane) unit from the plane that is defined by the C1, N1, C6, C7, and N2 atoms; i.e., the deviated distances of Ni atoms from the plane are 0.02 Å in **7a** and 0.41 Å in **8a**. Both **7a** and **8a** include an unsymmetrical coordination environment around the Ni center in their crystalline states, and the two olefin moieties are thus inequivalent. Nevertheless, the bond lengths of C2═C3 and C4═C5 are nearly identical, even when compared between **7a** and **8a**, i.e., C2═C3: 1.393(2) Å in **7a** and 1.380(8) Å in **8a**; C4═C5: 1.404(2) Å in **7a** and 1.402(7) Å in **8a**, implying a negligible variation of the electron density in these olefin moieties upon the aforementioned interconversion. However, an obvious elongation occurred in the bonds between the Ni and internal carbon atoms (C2 and C4), which should be caused by the structural constraint to adopt the distorted trigonal-planar geometry. The Ni−O1 bond (2.481(1) Å) is longer than the corresponding one in **2a** (2.227(1) Å),[14] whereas the participation of the bonding interaction between the Ni and O1 atoms in **7a** was confirmed by the AIM analysis (Figure S12).

We also found that ^{1}H NMR resonances of the coordinated olefin moieties, which are magnetically equivalent in solution at room temperature, upfield shifted upon the coordination change around the Ni center from four-coordinated **7a** to distorted trigonal-planar **8a** (Figure 6C). In the ^{31}P NMR

https://doi.org/10.1021/jacs.3c06267
J. Am. Chem. Soc. 2023, 145, 16938−16947

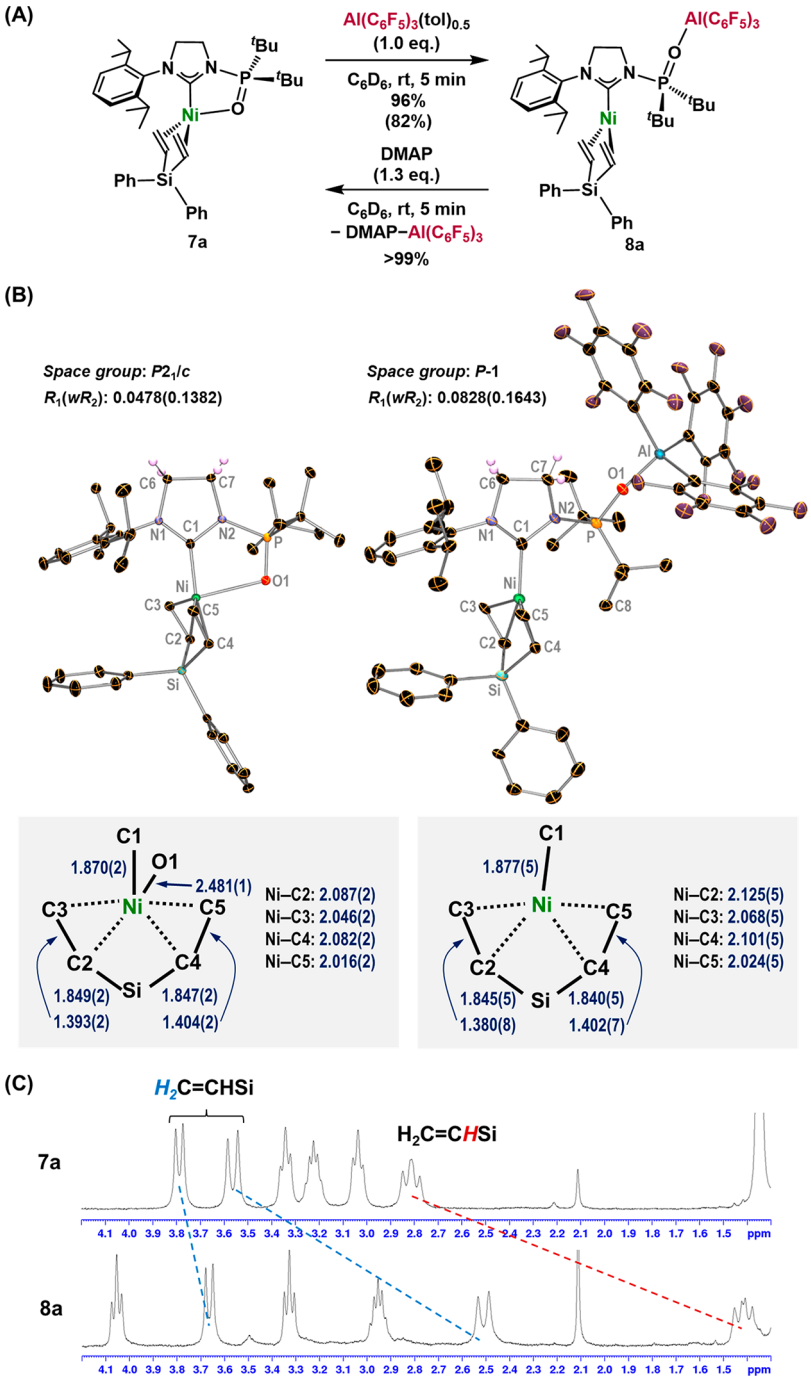

Figure 6. (A) Interconversion between **7a** and **8a** upon the addition and removal of $Al(C_6F_5)(tol)_{0.5}$. The yield was determined by NMR analyses. The yield of isolated products is shown in parentheses. (B) Molecular structure of **7a** (left) and **8a** (right) with thermal ellipsoids at 30% probability; H atoms (except those bound to C6 and C7) are omitted for clarity. Selected bond lengths (Å) are also shown. (C) The ^{1}H NMR spectra of **7a** and **8a** in C_6D_6.

spectrum, a significant downfield shift from δ_P 68.3 (**7a**) to 83.3 (**8a**) corroborates the formation of the P═O–Al bond. In their entirety, the results of the NMR and SC-XRD analyses suggest that the $Al(C_6F_5)_3$-mediated rotation of the *N*-phosphinoyl group can modulate not only the spatial environment around the Ni center but also the chemical environment surrounding the coordinated 1,4-diene unit through the interconversion between **7a** and **8a**.

CONCLUSIONS

In summary, we have reported a strategy that allows reversible modulation of the electronic state and spatial environment around metal centers that bear multifunctional ligands based on the use of Lewis acids. To this end, a series of *N*-phosphine oxide-substituted *N*-heterocyclic carbenes, referred to as (S)PoxIms, were employed, as (S)PoxIms can afford heterobimetallic species in κ-*C*-M^1 and κ-*O*-M^2 fashions without the formation of quenched NHC–Lewis acid adducts. The reaction between tetrahedral (*syn*-κ-*C*,*O*-(S)PoxIm)Ni-

https://doi.org/10.1021/jacs.3c06267
J. Am. Chem. Soc. 2023, 145, 16938–16947

$(CO)_2$ and $Al(C_6F_5)_3$ smoothly afforded heterobimetallic Ni/Al species such as trigonal-planar {κ-*C*-Ni$(CO)_2$}(μ-*anti*-(*S*)PoxIm){κ-*O*-Al$(C_6F_5)_3$} through complexation-induced rotation of the *N*-phosphine oxide moiety, while the addition of DMAP quantitatively triggered the formation of the former complex. We also confirmed that the interconversion between (*syn*-κ-*C*,*O*-SPoxIm)Ni(η^2:η^2-1,4-diene) and the corresponding heterobimetallic Ni/Al species effectively proceeded upon addition and removal of $Al(C_6F_5)_3$, which successfully demonstrates that the present strategy can be applied for modulating the spatial environment around not only metal centers but also the coordinated substrates. We experimentally and theoretically confirmed that the shape and size of the space around the Ni(0) center drastically expanded/contracted using this Lewis-acid-mediated procedure. Furthermore, a detailed discussion based on multinuclear NMR, IR absorption, and X-ray absorption spectroscopy shed light on the changes in the electronic states of the Ni centers. Thus, this work manifests a conceptually novel and effective approach to design and modulate the electronic and spatial environment surrounding metal centers in organometallic compounds using a combination of multifunctional ligands and Lewis acids.

■ ASSOCIATED CONTENT

Supporting Information

The Supporting Information is available free of charge at https://pubs.acs.org/doi/10.1021/jacs.3c06267.

Full details pertaining to the experimental methods, identification of the compounds, and DFT calculations. (PDF)

Accession Codes

CCDC 2263787−2263791, 2269436−2269437, and 2269439 contain the supplementary crystallographic data for this paper. These data can be obtained free of charge via www.ccdc.cam.ac.uk/data_request/cif, or by emailing data_request@ccdc.cam.ac.uk, or by contacting The Cambridge Crystallographic Data Centre, 12 Union Road, Cambridge CB2 1EZ, UK; fax: +44 1223 336033.

■ AUTHOR INFORMATION

Corresponding Authors

Yuta Uetake − *Department of Applied Chemistry, Faculty of Engineering, Osaka University, Suita, Osaka 565-0871, Japan; Innovative Catalysis Science Division, Institute for Open and Transdisciplinary Research Initiatives (ICS-OTRI), Osaka University, Suita, Osaka 565-0871, Japan;* orcid.org/0000-0002-4742-8085; Email: uetake@chem.eng.osaka-u.ac.jp

Sensuke Ogoshi − *Department of Applied Chemistry, Faculty of Engineering, Osaka University, Suita, Osaka 565-0871, Japan;* orcid.org/0000-0003-4188-8555; Email: ogoshi@chem.eng.osaka-u.ac.jp

Yoichi Hoshimoto − *Department of Applied Chemistry, Faculty of Engineering, Osaka University, Suita, Osaka 565-0871, Japan; Center for Future Innovation (CFi), Division of Applied Chemistry, Faculty of Engineering, Osaka University, Suita, Osaka 565-0871, Japan;* orcid.org/0000-0003-0882-6109; Email: hoshimoto@chem.eng.osaka-u.ac.jp

Authors

Yasuhiro Yamauchi − *Department of Applied Chemistry, Faculty of Engineering, Osaka University, Suita, Osaka 565-0871, Japan*

Yutaka Mondori − *Department of Applied Chemistry, Faculty of Engineering, Osaka University, Suita, Osaka 565-0871, Japan*

Yasuo Takeichi − *Department of Applied Physics, Graduate School of Engineering, Osaka University, Suita, Osaka 565-0871, Japan;* orcid.org/0000-0003-3334-0274

Takahiro Kawakita − *Department of Applied Chemistry, Faculty of Engineering, Osaka University, Suita, Osaka 565-0871, Japan*

Hidehiro Sakurai − *Department of Applied Chemistry, Faculty of Engineering, Osaka University, Suita, Osaka 565-0871, Japan; Innovative Catalysis Science Division, Institute for Open and Transdisciplinary Research Initiatives (ICS-OTRI), Osaka University, Suita, Osaka 565-0871, Japan;* orcid.org/0000-0001-5783-4151

Complete contact information is available at: https://pubs.acs.org/10.1021/jacs.3c06267

Notes

The authors declare no competing financial interest.

■ ACKNOWLEDGMENTS

We thank T. Honma (Japan Synchrotron Radiation Research Institute), S. Yamashita (High Energy Accelerator Research Organization), and H. Iwayama (Institute for Molecular Science) for their support of the XAS experiments. Ni K-edge XAS measurements were performed at the BL14B2 beamline of SPring-8 with the approval of the Japan Synchrotron Radiation Research Institute (proposal no. 2020A1871, 2021A1630, 2022A1767, and 2022A1784). Ni $L_{2,3}$-edge XAS measurements were performed at the BL-19B beamline of KEK under the approval of the Photon Factory Program Advisory Committee (proposal no. 2022P013), and at the BL4B beamline of the UVSOR Synchrotron Facility with the approval of Institute for Molecular Science (proposal no. 21-697). This project was supported by Grants-in-Aid for Scientific Research (C) (21K05070 to Y.H. and 22K05095 to Y.U.), Grants-in-Aid for Transformative Research Area (A) Digitalization-driven Transformative Organic Synthesis (22H05363 to Y.H.), and JST FOREST Program (JPMJFR2222 to Y.H.). Part of this work was supported by JST SPRING (grant JPMJSP2138 to Y.Y.). Part of the computation was performed using resources from the Research Center for Computational Science, Okazaki, Japan (Project: 22-IMS-C107).

■ REFERENCES

(1) Wu, K.; Doyle, A. G. Parameterization of phosphine ligands demonstrates enhancement of nickel catalysis via remote steric effects. *Nat. Chem.* **2017**, *9*, 779−784.

(2) Falivene, L.; Cao, Z.; Petta, A.; Serra, L.; Poater, A.; Oliva, R.; Scarano, V.; Cavallo, L. Towards the online computer-aided design of catalytic pockets. *Nat. Chem.* **2019**, *11*, 872−879.

(3) Durand, D. J.; Fey, N. Computational Ligand Descriptors for Catalyst Design. *Chem. Rev.* **2019**, *119*, 6561−6594.

(4) Zhang, Z.; Shao, Y.; Tang, J.; Jiang, J.; Wang, L.; Li, S. Supramolecular asymmetric catalysis mediated by crown ethers and related recognition systems. *Green Synth. Catal.* **2021**, *2*, 156−164.

(5) Trouvé, J.; Gramage-Doria, R. Beyond hydrogen bonding: recent trends of outer sphere interactions in transition metal catalysis. *Chem. Soc. Rev.* **2021**, *50*, 3565−3584.
(6) Blanco, V.; Leigh, D. A.; Marcos, V. Artificial switchable catalysts. *Chem. Soc. Rev.* **2015**, *44*, 5341−5370.
(7) Miller, A. J. M. Controlling ligand binding for tunable and switchable catalysis: cation-modulated hemilability in pincer-crown ether ligands. *Dalton Trans.* **2017**, *46*, 11987−12000.
(8) Yoo, C.; Dodge, H. M.; Miller, A. J. M. Cation-controlled catalysis with crown ether-containing transition metal complexes. *Chem. Commun.* **2019**, *55*, 5047−5059.
(9) Peris, E. Smart N-Heterocyclic Carbene Ligands in Catalysis. *Chem. Rev.* **2018**, *118*, 9988−10031.
(10) Braunstein, P.; Naud, F. Hemilability of Hybrid Ligands and the Coordination Chemistry of Oxazoline-Based Systems. *Angew. Chem., Int. Ed.* **2001**, *40*, 680−699.
(11) Fliedel, C.; Schnee, G.; Braunstein, P. Versatile coordination modes of novel hemilabile S-NHC ligands. *Dalton Trans.* **2009**, 2474−2476.
(12) Liang, Q.; Janes, T.; Gjergji, X.; Song, D. Iron complexes of a bidentate picolyl-NHC ligand: synthesis, structure and reactivity. *Dalton Trans.* **2016**, *45*, 13872−13880.
(13) Mondal, M.; Ranjeesh, T. K.; Gupta, S. K.; Choudhury, J. Labile coordination approach for the modulation of the electronic properties of ruthenium(II) and iridium(III) complexes within an "N-heterocyclic carbene (NHC)−pyridyl" dynamic platform. *Dalton Trans.* **2014**, *43*, 9356−9362.
(14) Yamauchi, Y.; Hoshimoto, Y.; Kawakita, T.; Kinoshita, T.; Uetake, Y.; Sakurai, H.; Ogoshi, S. Room-Temperature Reversible Chemisorption of Carbon Monoxide on Nickel(0) Complexes. *J. Am. Chem. Soc.* **2022**, *144*, 8818−8826.
(15) Hoshimoto, Y.; Kinoshita, T.; Ohashi, M.; Ogoshi, S. A Strategy to Control the Reactivation of Frustrated Lewis Pairs from Shelf-Stable Carbene Borane Complexes. *Angew. Chem., Int. Ed.* **2015**, *54*, 11666−11671.
(16) Hoshimoto, Y.; Ogoshi, S. Development of Metal Complexes Equipped with Structurally Flexible Carbenes. *Bull. Chem. Soc. Jpn.* **2021**, *94*, 327−338.
(17) For examples on LA-mediated reversible electronic modulation on metal centers, see: (a) Lee, B. Y.; Bazan, G. C.; Vela, J.; Komon, Z. J. A.; Bu, X. α-Iminocarboxamidato−Nickel(II) Ethylene Polymerization Catalysts. *J. Am. Chem. Soc.* **2001**, *123*, 5352−5353. (b) Kim, Y. H.; Kim, T. H.; Lee, B. Y.; Woodmansee, D.; Bu, X.; Bazan, G. C. α-Iminoenamido Ligands: A Novel Structure for Transition-Metal Activation. *Organometallics* **2002**, *21*, 3082−3084. (c) Hesp, K. D.; McDonald, R.; Ferguson, M. J.; Schatte, G.; Stradiotto, M. (κ^2-*P,S*)Pt(benzyl) complexes derived from 1/3-P^{i}Pr$_2$-2-S^{t}Bu-indene: facile synthesis of carbanion- and borate-containing zwitterions. *Chem. Commun.* **2008**, 5645−5647. (d) Hesp, K. D.; McDonald, R.; Ferguson, M. J.; Stradiotto, M. New Cationic and Zwitterionic Cp*M(κ^2-P,S) Complexes (M = Rh, Ir): Divergent Reactivity Pathways Arising from Alternative Modes of Ancillary Ligand Participation in Substrate Activation. *J. Am. Chem. Soc.* **2008**, *130*, 16394−16406. (e) Azoulay, J. D.; Rojas, R. S.; Serrano, A. V.; Ohtaki, H.; Galland, G. B.; Wu, G.; Bazan, G. C. Nickel α-Keto-β-Diimine Initiators for Olefin Polymerization. *Angew. Chem., Int. Ed.* **2009**, *48*, 1089−1092. (f) Azoulay, J. D.; Koretz, Z. A.; Wu, G.; Bazan, G. C. Well-Defined Cationic Methallyl α-Keto-β-Diimine Complexes of Nickel. *Angew. Chem., Int. Ed.* **2010**, *49*, 7890−7894. (g) Trofymchuk, O. S.; Gutsulyak, D. V.; Quintero, C.; Parvez, M.; Daniliuc, C. G.; Piers, W. E.; Rojas, R. S. *N*-Arylcyano-β-diketiminate Methallyl Nickel Complexes: Synthesis, Adduct Formation, and Reactivity toward Ethylene. *Organometallics* **2013**, *32*, 7323−7333. (h) Tseng, K. -N. T.; Kampf, J. W.; Szymczak, N. K. Regulation of Iron-Catalyzed Olefin Hydroboration by Ligand Modifications at a Remote Site. *ACS Catal.* **2015**, *5*, 411−415. (i) Lambic, N. S.; Brown, C. A.; Sommer, R. D.; Ison, E. A. Dramatic Increase in the Rate of Olefin Insertion by Coordination of Lewis Acids to the Oxo Ligand in Oxorhenium(V) Hydrides. *Organometallics* **2017**, *36*, 2042−2051. (j) Geri, J. B.; Shanahan, J. P.; Szymczak, N. K. Testing the Push-Pull Hypothesis: Lewis Acid Augmented N_2 Activation at Iron. *J. Am. Chem. Soc.* **2017**, *139*, 5952−5956. (k) Goudy, V.; Jaoul, A.; Cordier, M.; Clavaguéra, C.; Nocton, G. Tuning the Stability of Pd(IV) Intermediates Using a Redox Noninnocent Ligand Combined with an Organolanthanide Fragment. *J. Am. Chem. Soc.* **2017**, *139*, 10633−10636. (l) Shanahan, J. P.; Szymczak, N. K. Lewis Acid Effects on Calculated Ligand Electronic Parameters. *Organometallics* **2020**, *39*, 4297−4306. (m) Schmid, L.; Chábera, O.; Rüter, I.; Prescimone, A.; Meyer, F.; Yartsev, A.; Persson, P.; Wenger, O. S. Borylation in the Second Coordination Sphere of Fe^{II} Cyanido Complexes and Its Impact on Their Electronic Structures and Excited-State Dynamics. *Inorg. Chem.* **2022**, *61*, 15853−15863.
(18) For selected examples on LA-mediated ligand substitution reaction, see: (a) Liberman-Martin, A. L.; Levine, D. S.; Liu, W.; Bergman, R. G.; Tilley, T. D. Biaryl Reductive Elimination Is Dramatically Accelerated by Remote Lewis Acid Binding to a 2,2'-Bipyrimidyl-Platinum Complex: Evidence for a Bidentate Ligand Dissociation Mechanism. *Organometallics* **2016**, *35*, 1064−1069. (b) Warioba, C. S.; Jackson, L. G.; Neal, M. A.; Haines, B. E. Computational Study on the Role of Zn(II) Z-Type Ligands in Facilitating Diaryl Reductive Elimination from Pt(II). *Organometallics* **2023**, *42*, 16−26.
(19) For an example on proton-mediated electronic mudulation, see: Brennan, C.; Draksharapu, A.; Browne, W. R.; McGarvey, J. J.; Vos, J. G.; Pryce, M. T. Unexpected reversible pyrazine based methylation in a Ru(II) complex bearing a pyrazin-2'-yl-1,2,4-triazolato ligand and its effect on acid/base and photophysical properties. *Dalton Trans.* **2013**, *42*, 2546−2555.
(20) For examples on proton-mediated ligand alternation reaction, see: (a) Himeda, Y.; Onozawa-Komatsuzaki, N.; Sugihara, H.; Kasuga, K. Simultaneous Tuning of Activity and Water Solubility of Complex Catalysts by Acid-Base Equilibrium of Ligands for Conversion of Carbon Dioxide. *Organometallics* **2007**, *26*, 702−712. (b) Hashiguchi, B. G.; Young, K. J. H.; Yousufuddin, M.; Goddard, W. A., III; Periana, R. A. Acceleration of Nucleophilic CH Activation by Strongly Basic Solvents. *J. Am. Chem. Soc.* **2010**, *132*, 12542−12545. (c) Dixon, N. A.; McQuarters, A. B.; Kraus, J. S.; Soffer, J. B.; Lehnert, N.; Schweitzer-Stenner, R.; Papish, E. T. Dramatic tuning of ligand donor properties in (Ttz)CuCO through remote binding of H^+ (Ttz = hydrotris(triazolyl)borate). *Chem. Commun.* **2013**, *49*, 5571−5573.
(21) Acosta-Calle, S.; Miller, A. J. M. Tunable and Switchable Catalysis Enabled by Cation-Controlled Gating with Crown Ether Ligands. *Acc. Chem. Res.* **2023**, *56*, 971−981.
(22) van der Ham, A.; Hansen, T.; Lodder, G.; Codée, J. D. C.; Hamlin, T. A.; Filippov, D. V. Computational and NMR Studies on the Complexation of Lithium Ion to 8-Crown-4. *ChemPhysChem* **2019**, *20*, 2103−2109.
(23) Ouyang, G.-H.; He, Y.-M.; Li, Y.; Xiang, J.-F.; Fan, Q.-H. Cation-Triggered Switchable Asymmetric Catalysis with Chiral Aza-CrownPhos. *Angew. Chem., Int. Ed.* **2015**, *54*, 4334−4337.
(24) Asada, T.; Hoshimoto, Y.; Ogoshi, S. Rotation-Triggered Transmetalation on a Heterobimetallic Cu/Al *N*-Phosphine-Oxide-Substituted Imidazolylidene Complex. *J. Am. Chem. Soc.* **2020**, *142*, 9772−9784.
(25) Branzi, L.; Baron, M.; Armelao, L.; Rancan, M.; Sgarbossa, P.; Graiff, C.; Pöthig, A.; Biffis, A. Coordination chemistry of gold with *N*-phosphine oxide-substituted imidazolylidenes (POxIms). *New J. Chem.* **2019**, *43*, 17275−17283.
(26) Dorta, R.; Stevens, E. D.; Hoff, C. D.; Nolan, S. P. Stable, Three-Coordinate Ni(CO)$_2$(NHC) (NHC = *N*-Heterocyclic Carbene) Complexes Enabling the Determination of Ni-NHC Bond Energies. *J. Am. Chem. Soc.* **2003**, *125*, 10490−10491.
(27) Dorta, R.; Stevens, E. D.; Scott, N. M.; Costabile, C.; Cavallo, L.; Hoff, C. D.; Nolan, S. P. Steric and Electronic Properties of N-Heterocyclic Carbenes (NHC): A Detailed Study on Their Interaction with Ni(CO)$_4$. *J. Am. Chem. Soc.* **2005**, *127*, 2485−2495.
(28) A set of (R_a) and (S_a) atropisomers of **3a** were identified in the asymmetric unit of the single crystal, as bulky Al(C$_6$F$_5$)$_3$ would inhibit

https://doi.org/10.1021/jacs.3c06267
J. Am. Chem. Soc. 2023, 145, 16938−16947

the rotation of the *N*-phosphinoyl moiety upon complexation and induce N−P axial chirality. For details on complexation-induced N−P axial chirality, see: (a) Kinoshita, T.; Sakuraba, M.; Hoshimoto, Y.; Ogoshi, S. Complexation between MOTf (M = Li and Na) and *N*-Phosphine Oxide-substituted Imidazolylidenes via Coordination of the *N*-Phosphoryl Group. *Chem. Lett.* **2019**, *48*, 230−233. (b) Asada, T.; Hoshimoto, Y.; Kawakita, T.; Kinoshita, T.; Ogoshi, S. Axial Chirality around N-P Bonds Induced by Complexation between $E(C_6F_5)_3$ (E = B, Al) and an *N*-Phosphine Oxide-Substituted Imidazolinylidene: A Key Intermediate in the Catalytic Phosphinoylation of CO_2. *J. Org. Chem.* **2020**, *85*, 14333−14341. (c) Hoshimoto, Y.; Yamauchi, Y.; Terada, T.; Ogoshi, S. Complexation-Induced N-P Axial Chirality in Sm(II) *N*-Phosphine-Oxide-Substituted Imidazolylidene and Imidazolinylidene Complexes. *Can. J. Chem.* **2023**, *101*, 429−433.

(29) Kumar, P S. V.; Raghavendra, V.; Subramanian, V. Bader's Theory of Atoms in Molecules (AIM) and its Applications to Chemical Bonding. *J. Chem. Sci.* **2016**, *128*, 1527−1536.

(30) Macchi, P.; Sironi, A. Chemical bonding in transition metal carbonyl clusters: complementary analysis of theoretical and experimental electron densities. *Coord. Chem. Rev.* **2003**, *238*−*239*, 383−412.

(31) He, W.; Beattie, D. D.; Zhou, H.; Bowes, E. G.; Schafer, L. L.; Love, J. A.; Kennepohl, P. Direct metal−carbon bonding in symmetric bis(C−H) agostic nickel(I) complexes. *Chem. Sci.* **2021**, *12*, 15298−15307.

(32) Bistoni, G.; Rampino, S.; Scafuri, N.; Ciancaleoni, G.; Zuccaccia, D.; Belpassi, L.; Tarantelli, F. How π back-donation quantitatively controls the CO stretching response in classical and nonclassical metal carbonyl complexes. *Chem. Sci.* **2016**, *7*, 1174−1184.

(33) Gómez-Suárez, A.; Nelson, D. J.; Nolan, S. P. Quantifying and understanding the steric properties of N-heterocyclic carbenes. *Chem. Commun.* **2017**, *53*, 2650−2660.

(34) Heully, J.-L.; Lindgren, I.; Lindroth, E.; Lundqvist, S.; Mårtensson-Pendrill, A.-M. Diagonalisation of the Dirac Hamiltonian as a basis for a relativistic many-body procedure. *J. Phys. B: At. Mol. Phys.* **1986**, *19*, 2799−2815.

(35) Chang, C.; Pelissier, M.; Durand, P. Regular Two-Component Pauli-Like Effective Hamiltonians in Dirac Theory. *Phys, Scr.* **1986**, *34*, 394−404.

(36) van Lenthe, E.; Baerends, E. J.; Snijders, J. G. Relativistic regular two-component Hamiltonians. *J. Chem. Phys.* **1993**, *99*, 4597−4610.

(37) DiMucci, I. M.; Lukens, J. T.; Chatterjee, S.; Carsch, K. M.; Titus, C. J.; Lee, S. J.; Nordlund, D.; Betley, T. A.; MacMillan, S. N.; Lancaster, K. M. The Myth of d^8 Copper(III). *J. Am. Chem. Soc.* **2019**, *141*, 18508−18520.

(38) A bonding interaction between $Ni(CO)_4$ and Lewis-acidic centers at the surface of γ-Al_2O_3 has already been investigated; for details, see: Rao, K. M.; Spoto, G.; Zecchina, A. IR Investigation of $Ni(CO)_4$ Interaction with Silicalite, ZSM-5, Zeolite-Y, and γ -Al_2O_3. *Langmuir* **1989**, *5*, 319−325.

(39) For the isolation of a Ni complex including a CO−Li^+ interaction, see: Hou, H.; Rheingold, A. L.; Kubiak, C. P. An Anionic Zerovalent Nickel Carbonyl Complex Supported by a Triphosphine Borate Ligand: An Ni-C≡O-Li Isocarbonyl. *Organometallics* **2005**, *24*, 231−233.

(40) For the formation of Lewis adducts between M−CO units and Lewis-acidic species, see: (a) Kotz, J. C.; Turnipseed, C. D. Evidence for the Interaction of Trimethylalane with the Oxygen Atom of a Terminal Metal Carbonyl Group. *Chem. Commun.* **1970**, 41−42. (b) Burlitch, J. M.; Petersen, R. B. Variable site of Lewis basicity of π-$C_5H_5W(CO)_3^-$ in complexes with $(C_6H_5)_3In$ and $(C_6H_5)_3Al$. *J. Organomet. Chem.* **1970**, *24*, C65−C67. (c) Petersen, R. B.; Stezowski, J. J.; Wan, C.; Burlitch, J. M.; Hughes, R. E. A Novel Metal-Carbonyl-Metal Bonding System. Synthesis and Stereochemistry of $Al[W(CO)_3C_5H_5]_3(C_4H_8O)_3$. *J. Am. Chem. Soc.* **1971**, *93*, 3532−3533. (d) Ulmer, S. W.; Skarstad, P. M.; Burlitch, J. M.; Hughes, R. E. Synthesis, Stereochemistry, and Bonding of Tetrapyridinemagnesium(II) Bis(π-cyclopentadienyltricarbonylmolybdate(-I)) and Related Compounds. *J. Am. Chem. Soc.* **1973**, *95*, 4469−4471. (e) Darensbourg, M. Y.; Jimenez, P.; Sackett, J. R.; Hanckel, J. M.; Kump, R. L. Interactions of $CpM'(CO)_3^-$ (M' = Cr, Mo, W) with Cations: Effects on CO Exchange and RX Addition Reactions. *J. Am. Chem. Soc.* **1982**, *104*, 1521−1530. (f) Zhuang, B.; Sun, H.; He, L.; Zhou, Z.; Lin, C.; Wu, K.; Huang, Z. Synthesis, structure and possible formation pathway of a novel cobalt carbonyl compound with new type B-O bond, $Co(CO)_3(PPh_3)_2BEt_3$, and mixed metal Co-Fe-S cluster with possible nonlinear optical property, $[Et_4N][CoFe_2(CO)_8S(PPh_3)]$. *J. Organomet. Chem.* **2002**, *655*, 233−238. (g) García, F.; Hopkins, A. D.; Kowenicki, R. A.; McPartlin, M.; Rogers, M. C.; Silvia, J. S.; Wright, D. S. Syntheses and Structure of Heterometallic Complexes Containing Tripodal Group 13 Ligands $[RE(2\text{-py})_3]^-$ (E = Al, In). *Organometallics* **2006**, *25*, 2561−2568. (h) Fuchs, J.; Irran, E.; Hrobárik, P.; Klare, H. F. T.; Oestreich, M. Si-H Bond Activation with Bullock's Cationic Tungsten(II) Catalyst: CO as Cooperating Ligand. *J. Am. Chem. Soc.* **2019**, *141*, 18845−18850. (i) Tinnermann, H.; Sung, S.; Csókás, D.; Toh, Z. H.; Fraser, C.; Young, R. D. Alkali Metal Adducts of an Iron(0) Complex and Their Synergistic FLP-Type Activation of Aliphatic C-X Bonds. *J. Am. Chem. Soc.* **2021**, *143*, 10700−10708. (j) Fritz, M.; Demeshko, S.; Würtele, C.; Finger, M.; Schneider, S. Linearly Bridging N_2 versus CO: Chemical Bonding and Spin-Controlled Reactivity. *Eur. J. Inorg. Chem.* **2023**, *26*, No. e202300011.

https://doi.org/10.1021/jacs.3c06267
J. Am. Chem. Soc. 2023, 145, 16938−16947